



ELSEVIER

Available online at www.sciencedirect.com

SCIENCE @ DIRECT®

Nuclear Instruments and Methods in Physics Research A 496 (2003) 8–25

**NUCLEAR
INSTRUMENTS
& METHODS
IN PHYSICS
RESEARCH**
Section A

www.elsevier.com/locate/nima

A fast non-ferric kicker for the muon ($g - 2$) experiment

Efstathios Efstathiadis^a, Y.Y. Lee^b, Jian-lin Mi^b, Chien Pai^b, Jonathan M. Paley^a,
B. Lee Roberts^{a,*}, Ralph T. Sanders^b, Yannis K. Semertzidis^b,
David S. Warburton^b

^aDepartment of Physics, Boston University, Boston, MA 02215, USA

^bBrookhaven National Laboratory, Upton, NY 11973, USA

Received 1 April 2002; received in revised form 17 July 2002; accepted 25 July 2002

Abstract

A fast, non-ferric kicker has been designed, built and installed in the muon ($g - 2$) experiment at the Brookhaven Alternating Gradient Synchrotron. A current pulse of 4200 A peak, and base-width of 400 ns, is passed in opposite directions through parallel plates 10 cm apart on either side of the muon storage region in the ($g - 2$) storage ring. A field integral of 0.1 Tm was achieved, which kicks the 3.09 GeV/ c muon beam by about 10 mrad. This kick is achieved by employing three identical 1.76 m long sections, each powered by a separate pulse-forming network. The design and performance of the kicker is presented.

© 2003 Elsevier Science B.V. All rights reserved.

PACS: 29.27.Ac

Keywords: Fast non-ferric kicker; Muon $g - 2$

1. Introduction

A new experiment to measure the anomalous g -value of the muon, a_μ , a factor of 20 times more precisely than the last CERN ($g - 2$) experiment, [1], began construction at the Brookhaven AGS in 1988 [2,3]. The ultimate goal is a relative error on a_μ of ± 0.35 parts per million (ppm). The central element to achieving the data rate needed to obtain a factor of 200 in statistics over the CERN experiments [1] is the direct injection of muons into the storage ring by means of a fast muon

kicker.¹ In the third CERN experiment [1] and in the first run in 1997 at Brookhaven [2], a bunched pion beam was injected into the storage ring, and muons were kicked onto stable orbits by the decay $\pi^+ \rightarrow \mu^+ \nu_\mu$. In mid-1998 the fast kicker described in this paper became operational, and subsequent measurements [3] were made using direct muon injection into the storage ring.

For polarized muons moving in a uniform magnetic field \vec{B} which is perpendicular to the muon spin direction and to the plane of the orbit, and with an electric quadrupole field \vec{E} for vertical

*Corresponding author.

E-mail address: roberts@bu.edu (B.L. Roberts).

¹ The idea of direct muon injection was first proposed by Fred Combley at a workshop held at Brookhaven in 1984.

focusing [1,4], the difference angular frequency ω_a , between the spin precession frequency ω_s and the cyclotron frequency ω_c , is given by

$$\vec{\omega}_a = -\frac{e}{m_\mu} \left[a_\mu \vec{B} - \left(a_\mu - \frac{1}{\gamma_\mu^2 - 1} \right) \vec{\beta} \times \vec{E} \right] \quad (1)$$

which is the frequency the muon spin precesses relative to the momentum vector. The dependence of ω_a on the electric field is eliminated (to lowest order) by storing muons with the “magic” $\gamma_\mu = 29.3$, which corresponds to a muon momentum $p_\mu = 3.09 \text{ GeV}/c$. Hence measurement of ω_a and of B determines a_μ .

The use of electrostatic quadrupoles permits us to have a very uniform magnetic field, which can be monitored and measured to about 0.1 ppm accuracy using NMR techniques [5]. The magnetic field in the storage ring is mapped by an NMR trolley which travels in the (evacuated) vacuum chamber. The trolley is a cable-car with a matrix of 17 NMR probes, which maps the magnetic field in the muon storage region. One of the trolley cables is a standard co-axial cable which provides both power and communication to the trolley.

In our experiment, positrons from the in-flight decay $\mu^+ \rightarrow e^+ \nu_e \bar{\nu}_\mu$ are detected with Pb-scintillating fiber calorimeters placed symmetrically at 24 positions around the inside of the storage ring [6]. The time spectrum of the positrons forms the signal from which the value of ω_a and hence a_μ is extracted.

The pion injection technique permitted a sufficient number of muons to be stored in a ring to make a 7.3 ppm measurement at CERN, and a 13 ppm measurement was made in a brief run at the Brookhaven AGS [2]. This 13 ppm measurement illuminated the difficulties in going beyond the few ppm level without a new technique. The principal limitations were the small number of muons stored per injected pion ($\sim 5 \times 10^{-5}$), and the background flash in the detectors caused by pions which do not produce stored muons interacting in the storage ring yoke and other material.

Well before this first test run, it became clear that direct muon injection would be necessary in order to achieve the needed factor of 200 in statistics over the CERN experiment

(see footnote 1). Monte Carlo studies showed that a factor of ten increase in the number of muons stored per fill of the ring might be achieved with direct muon injection, and background studies with a pulsed beam indicated that the flash which accompanies the filling of the ring would be reduced by a factor of 50.

The precision magnetic field produced by the storage ring put severe restrictions on the kicker design. The storage ring magnet is a super-ferric 700 ton, 14 m diameter circular “C”-magnet, with the opening facing inward toward the ring center [7]. The field is excited by three 14 m diameter superconducting coils which carry 5.2 kA to produce the 1.45 T magnetic field. The field is now shimmed to be uniform to ± 1 ppm when integrated over azimuth. Thus unlike conventional storage rings, the $(g-2)$ ring is essentially a monolithic structure, with discontinuities of $160 \mu\text{m}$ every 1.9 m in the pole pieces, and a minimum of holes in the back-leg of the magnet yoke. A plan view of the incoming beam, the inflector magnet and the storage ring is shown in Fig. 1.

The geometry of the pole pieces, and the exit of the superconducting inflector is shown in Fig. 2. The usual technique of matching apertures (and phase space) is impossible in this setting. The beam enters through a hole in the back-leg of the magnet, and enters a superconducting inflector magnet [8], 1.7 m in length placed between the hole in the back of the yoke and the edge of the muon storage region. This superconducting iron free septum magnet substantially cancels the 1.45 T storage ring field and delivers the beam approximately parallel to the central orbit, but 77 mm further out in radius.

In our beamline design [9], we allowed for either a muon or pion beam to be brought to the inflector entrance. Muons are produced by pion decay in the 72 m straight transport channel and one can select pions or muons with a momentum slit near the end of the beam line. If the injection momentum is set to the beamline momentum, a pion beam is selected. If it is set 1–2% lower, a muon beam with a small pion tail is selected.

The electrostatic quadrupoles are arranged in the ring with a four-fold symmetry, as shown

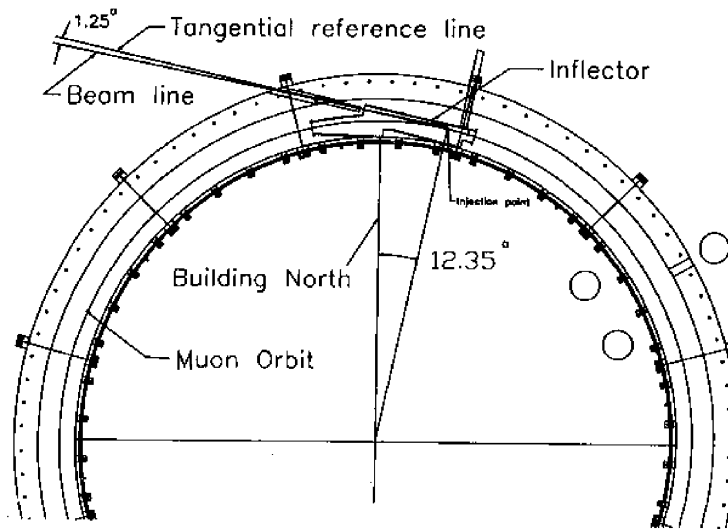


Fig. 1. The inflector-storage ring geometry. The magnet yoke consists of 12 sections held together mechanically to form a single monolithic whole.

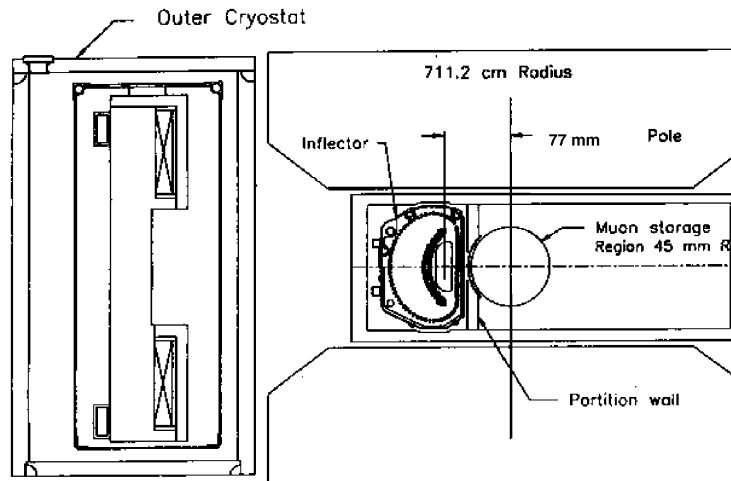


Fig. 2. The inflector exit-vacuum chamber geometry. The center of the storage ring is to the right. The gap between the pole pieces is 180 mm, and the inflector exit is $18 \times 56 \text{ mm}^2$ (ignoring the chamfer on the outer radius corners).

below in Fig. 3, making it a weak focusing storage ring with field index $n \approx 0.137$. The vacuum chamber is made up of 12 scalloped sections connected by bellows, with each of the sections having two scallops. The 24 electron/positron detector assemblies sit on the tracks indicated in the figure, with the detector placed behind the radial windows made by the scallop. The quadrupoles

occupy one and a half vacuum chambers, covering 43% of the ring.

Direct muon injection into the storage ring is accomplished by giving the muon beam a kick at a quarter of a betatron wavelength around from the inflector. An estimate of the kick needed can be obtained from the geometry shown in Fig. 4. The beam enters at $\theta = 0$ on a circle centered a distance

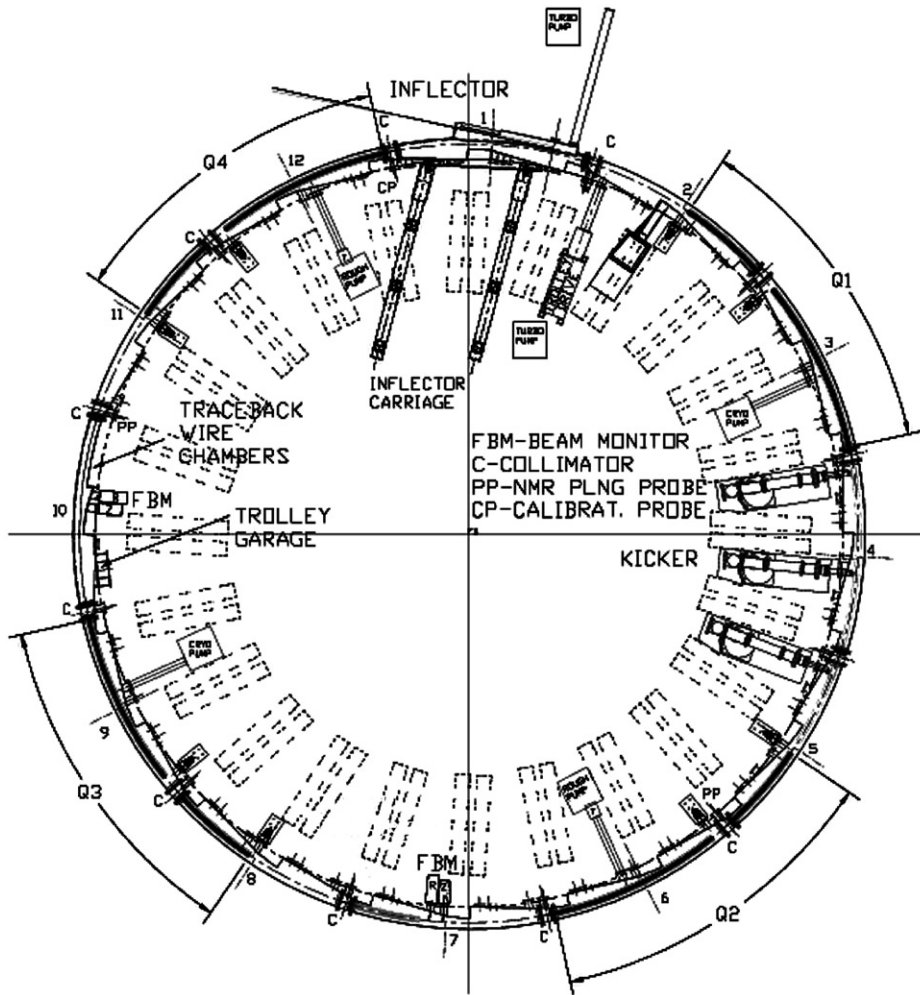


Fig. 3. The layout of the storage ring showing the location of the inflector, the kicker and the quadrupoles (which are labeled Q1–Q4). The scalloped vacuum chamber consists of 12 sections joined by bellows. The chambers containing the inflector, the NMR trolley garage, and the trolley drive mechanism were special chambers. The other chambers were standard, with either quadrupole or kicker assemblies installed inside. The 24 pairs of dashed rectangles are the supports for the detector assemblies.

$x_c = 77$ mm from the geometric center of the ring. The angle β is 10.8 mrad. One needs a field integral of ~ 0.1 Tm to achieve this kick.

While electric, magnetic and combination electromagnetic kickers were considered, we settled on a magnetic kicker design. The length of the kicker is limited by the space between the electrostatic quadrupoles, about 5 m. The necessity for keeping the inductance of the whole system low to maximize the peak current, made the design challenging. Because of the very stringent require-

ments on the storage ring magnetic field uniformity, no magnetic materials could be used. Thus the kicker field had to be generated and shaped solely with currents. Even with the kicker field generated by currents, there existed the potential problem of inducing eddy currents which might affect the magnetic field which is seen by the stored muons.

The basic kicker design uses two parallel current sheets with cross-overs at each end so that the current goes in opposite directions in the two

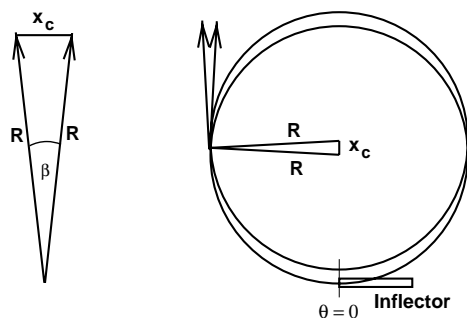


Fig. 4. A Sketch of the beam geometry. $R = 7112$ mm is the storage ring radius, $x_c = 77$ mm is the distance between the inflector center and the center of the storage region. This is also the distance between the centers of the circular trajectory a particle entering at the inflector center (at $\theta = 0$ with $x' = 0$) will follow, and the circular trajectory a particle at the center of the storage volume (at $\theta = 0$ with $x' = 0$) will follow.

plates. Alternately this geometry could be viewed as a single current loop.

Initial calculations for a somewhat idealized ring estimated that up to a third of the muons transported through the inflector would be stored. For the actual storage ring with the present inflector geometry, the electrostatic quadrupole system and π/μ beam transport system, tracking calculations indicated that a maximum of 8.3% injection efficiency is achievable. This efficiency would permit on the order of a factor of ten more muons to be stored per fill with direct muon injection when compared to pion injection.

Another potential problem of direct muon injection (mentioned above) is that one must understand any residual magnetic field (RMF) from the kicker due to eddy currents, since this RMF could be large enough to change the average field seen by the muons. The magnetic field must be stable over the short term to 0.1 ppm, and must be known to 0.1 ppm.

2. Kicker design

2.1. General considerations

The geometry and magnetic field requirements of the $(g - 2)$ storage ring place severe restrictions

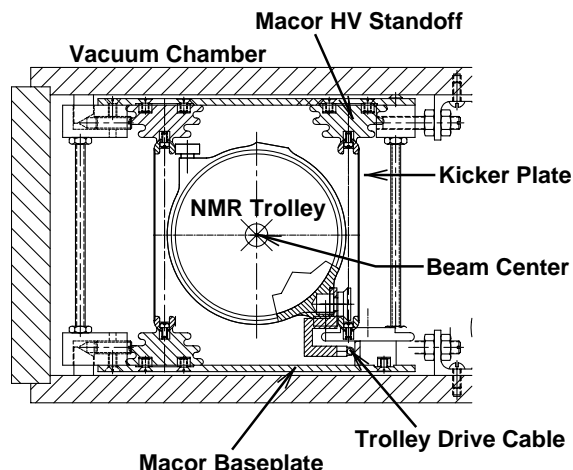


Fig. 5. The geometry inside the kicker vacuum chamber. Only three of the four sides of the vacuum chamber are shown; the inner radius (right-hand) side is missing. The kicker electrodes are shown supporting the NMR trolley (the body of which has a circular cross-section). The fixture on the lower right (at 4:00 on the trolley body) supports the forces needed to move the trolley, and the cable is attached to the bottom of this “C” shaped fixture. The high-voltage standoffs are made of macor, as are the top and bottom plates which have recessed holes to secure the standoffs. The top and bottom plates, along with the vertical supports and the kicker electrode-standoff assembly form a rigid cage assembly. The kicker plates are 80 mm (with rails 94 mm) high, 1760 mm long, 0.75 mm thick. The plates are 102.24 mm apart. The NMR trolley diameter is 88 mm.

on the kicker design. We cannot tolerate any iron or stainless steel near the storage region, so the high-voltage feed-through is ceramic and titanium, and all other parts are aluminum (with brass and plastic hardware), including the magnet electrodes. The space between the pole tips limits the plate height, and the need to have plates as tall as possible presents high-voltage stand-off issues inside the vacuum chamber (see Fig. 5). The need for the passage of the NMR trolley through the kicker vacuum chambers means that the kicker plates have to have rails on them which are robust enough to support the trolley, which has a mass of ~ 2 kg.

Because of the high voltages involved, the pulse-forming network and resonant charging circuit are in a vessel filled with Dow-Corning 561 silicon dielectric fluid. The kicker magnet is in the beam vacuum chamber, with a HV feed-through going

from oil to vacuum. To reduce the risk of contaminating the vacuum chamber with oil in the result of a mechanical failure of the HV feed-through, a buffer region containing fluorinert (3M FC40 fluorocarbon) was placed between the oil tank and the vacuum chamber. See Fig. 8 for the location of the feed-through.

The small space between the pole pieces, the location of the superconducting magnet's yoke and coils, and the constraint in azimuth placed by the 24 detector stations means that the kicker pulse-forming network must be placed radially inward from the magnet connection. The three kicker sections are placed at about 90° around the ring from the inflector end.

The injected beam pulse provided by the AGS has a base-width of about 130 ns ($\sigma \approx 25$ ns). The initial design called for a peak current of ~ 7000 A, which was to be provided by a slightly underdamped LR circuit, with a base-width on the current pulse of about 250 ns. In reality, we were limited by the system inductance, and were only able to achieve ~ 400 ns base-width. Thus the muon beam is kicked several times before the pulse dies away.

The ideal kicker current pulse is a step function wider than the time-width of the beam, but less than the cyclotron period of 149 ns. In reality we were limited to a current waveform generated by an underdamped LCR circuit.

To keep the inductance of a single assembly at a reasonable value, it was necessary to divide the

kicker magnet into three identical 1.76 m long sections, each driven by a separate pulse-forming network (modulator). With the inductance and resistance obtained from the physical assembly (including the thyatron), each modulator delivers a current pulse of approximately 4200 A, with an initial voltage of 95 kV on the capacitor.

2.2. Electrical design

The pulse-forming network is a simple LCR circuit. The capacitor is charged resonantly and then discharged through a resistor to ground by firing an English Electric Valve (EEVCX1699) deuterium thyatron. The other side of the capacitor is connected to the kicker electrode assembly inside of the vacuum chamber.

2.2.1. The simple modulator circuit

The simple LCR circuit is shown in Fig. 6. The current on the plates is of the form

$$I(t) = I_0 e^{(-\gamma/2)t} \sin(2\pi f_d t + \phi_d) \quad (2)$$

where

$$f_d = \frac{1}{2\pi} \left(\frac{1}{LC} \right)^{1/2} \left\{ 1 - \frac{R^2 C}{4L} \right\}^{1/2} = \frac{1}{2\pi} \sqrt{\frac{1}{LC} - \frac{R^2}{4L^2}} \quad (3)$$

and the width and peak current are given by

$$\gamma = \frac{R}{L} \quad \text{and} \quad I_0 = \frac{V_0}{2\pi f_d L} \quad (4)$$

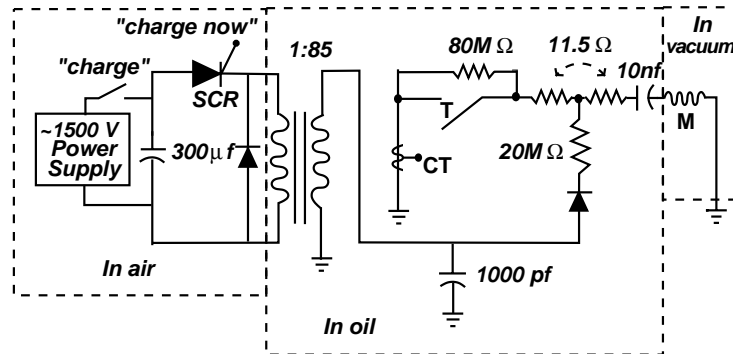


Fig. 6. The (Ideal) circuit of the Kicker. Stray inductance and capacitance are not shown. The inductor labeled M represents the kicker magnet; T represents an English Electric Valve deuterium thyatron; CT is a current transformer which gives the current waveform.

Table 1

The values of the elements and some properties of the simple circuit. Note that the 1.6 μH inductance is the estimated inductance of the whole kicker circuit. τ_0 is the undamped period, τ_d is the damped period, and τ is the decay time of the waveform

Quantity	Value	Quantity	Value
R	11.5 Ω	L	$\sim 1.6 \mu\text{H}$
C	10 nF		
f_0	$1.258 \times 10^6 \text{ Hz}$	τ_0	795 ns
γ	$8.06 \times 10^6 \text{ s}^{-1}$	$\tau = \frac{2L}{R}$	248 ns
f_d	$1.082 \times 10^6 \text{ Hz}$	τ_d	924.3 ns

The values of these parameters for our simple LCR circuit are given in Table 1. For critical damping, $R_{\text{Critical}} = 25.3 \Omega$.

2.2.2. Inductance and capacitance calculations and measurements

In the design phase, the inductance of each kicker component was calculated with OPERA. The calculated inductance of the various components is given below in Table 2, and the total calculated inductance of the magnet-feed-through system is 1.00 μH .

A prototype vacuum chamber and kicker electrode assembly was constructed which was a replica of the full design, except for being straight rather than having the storage ring radius of curvature. Measurements of the inductance and capacitance of the prototype kicker assembly were made with a Hewlett–Packard network analyzer, and the results are given in Table 3.

While the measured inductance of 1.2 μH is close to the calculated inductance of 1.0 μH , from the waveform produced by the full circuit the inductance of the entire assembly was estimated to be $\sim 1.6 \mu\text{H}$. Our guess is that most of this additional inductance is contributed by the thyatron and stray inductance from the full setup, which were not included in the measurements. A simple estimate of the thyatron inductance which assumed the thyatron to be a coaxial line gave 0.2–0.3 μH , consistent with this hypothesis.

Table 2

Calculated inductances for kicker elements. The inductance of the kicker plates was calculated with OPERA, the inductance of the connector was calculated, and the feed-through inductance was measured

Component	Inductance (μH)
Kicker plates	0.58
Connector	0.07
HV feed-through	0.35
Total calculated inductance	1.00

Table 3

The measured values of the prototype circuit elements

System	L (μH)	R (Ω)	C (nF)
Magnet-connector-feed-through	0.92		
Resistor-capacitor	0.273	11.9	10.2
Full system	1.2	11.9	10.1

2.3. Mechanical design

The configuration of how the system fits into the magnet gap is given in Fig. 7. The center of the storage volume is shown by a cross in the middle of the region between the pole pieces. The gap between the pole pieces is 180 mm, and the muon storage region is a 90 mm diameter circle.

A cut-away view of the modulators is shown in Fig. 8. The charging supply is connected in the middle of the resistor stack. In Fig. 5 the layout inside the beam vacuum chamber is shown. The kicker plates are electron-beam welded to rails, which also serve the function of eliminating sharp edges (and thus breakdown).

2.4. The measured current waveform

The current waveform and resulting magnetic field were measured for the prototype magnet. In Fig. 6 a current transformer is shown on the ground side of the thyatron. While this current waveform should be the same as that through the magnet, in the R&D stage we placed a second

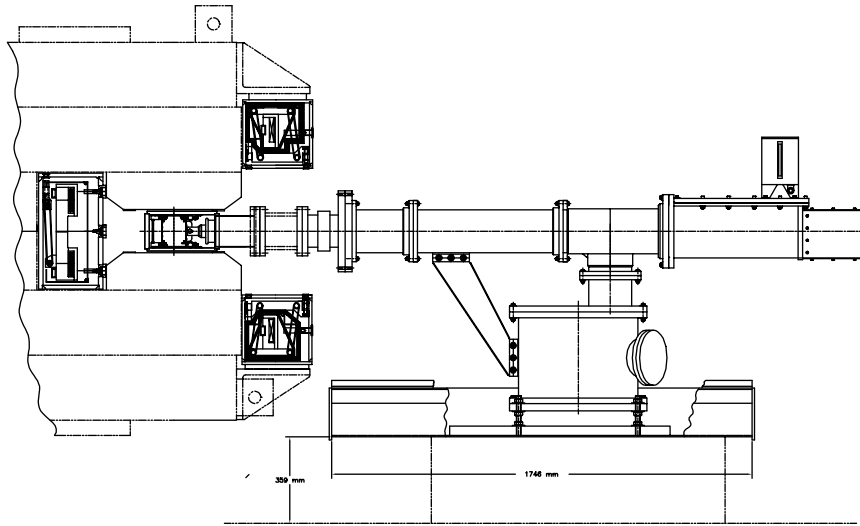


Fig. 7. Sideview of the kicker assembly and the storage ring magnet. The magnet and modulator support structure is not shown. The vertical line between the pole pieces is at the central orbit radius of 7112 mm.

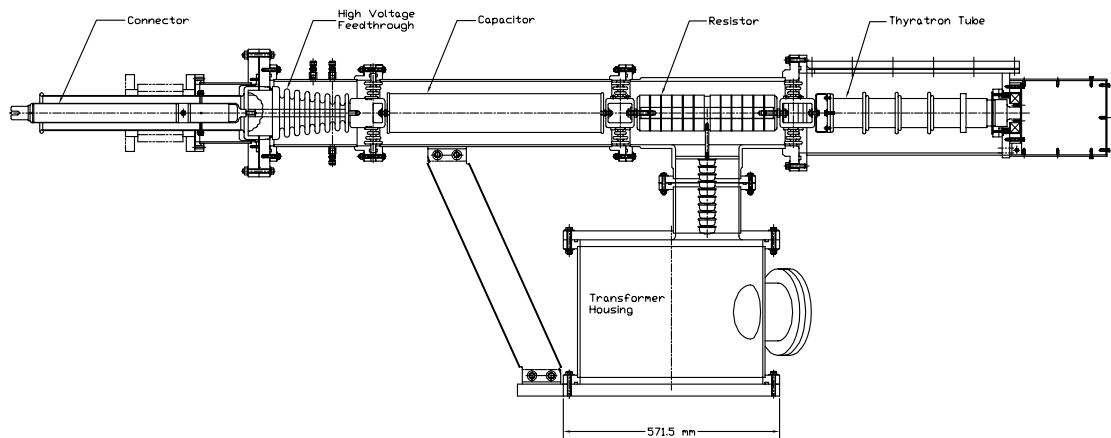


Fig. 8. A side view of the modulator showing the location of the resistor stack, the capacitor, thyatron tube, and the high-voltage feed-through. The connector carries the high current to the kicker plates. The region around the high-voltage feed-through is filled with SF40, rather than oil. Provisions to reverse the connection (to store the opposite polarity muons) are provided.

current transformer on the ground side of the magnet to confirm this assumption. As was expected, the two waveforms were essentially identical. The measured waveform from the prototype along with a simple LCR circuit pulse shape are shown in Fig. 9.

In Fig. 10 the current pulses from each of the three modulators in the storage ring are shown along with the pulse from a fast scintillator which was placed in the incoming beam thus giving the

time distribution of the beam incident on the storage ring.

3. Calculations of the kicker magnetic field and eddy currents

The static and time varying fields have been calculated for the prototype kicker configuration

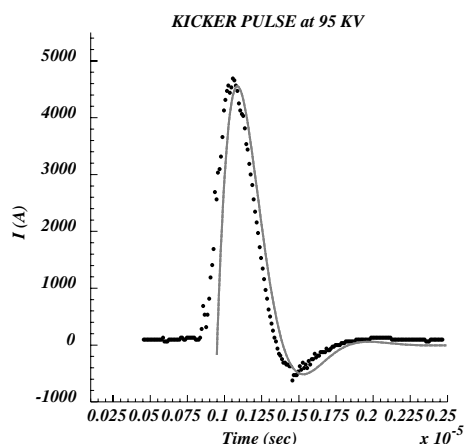


Fig. 9. The measured kicker waveform at 95 kV in the prototype setup. The line is an LCR waveform that matches the measurement. In this prototype version, a spark gap (rather than a thyatron) was used to discharge the capacitor.

using the package OPERA 2d,² and are shown below in Figs. 11 and 12.

We have used the OPERA 2-d transient analysis software package (see footnote 2) to simulate the magnetic field distribution during the kicker pulse. We optimized the material of the kicker plates, their thickness, and geometry to minimize the residual eddy currents $\geq 20 \mu\text{s}$ after the muon injection time. The material of choice for the plates is aluminum with the vertical thin part having a thickness of 0.75 mm. The vertical magnetic field distribution over one-quarter of the kicker cross-section is shown in Fig. 11.

The aluminum resistivity used in the model is $4.1 \times 10^{-8} \Omega\text{m}$ the same as that of the commercial grade aluminum (Al6061-T6) used in the construction of the kicker plates. For a typical peak current of 4000 A, one calculates a field of about 140 G at the center of the muon storage region (lower left corner of Fig. 11). The presence of the vacuum chamber reduces the peak magnetic field by about 20% for a current pulse of about 400 ns base-width due to eddy currents from the top/bottom plates of the vacuum chamber. This influences the

field distribution, lowering the field near the top/bottom plates of the vacuum chamber (see Figs. 11 and 12) and reducing the kick given to muons in the top and bottom of the beam. The magnetic field near the plates is highly inhomogeneous and much higher than at the center, as can be seen in Figs. 11 and 12.

In the design stage, no specifications were placed on the field quality, except that it be adequate to permit a reasonable number of muons be stored. Because of the geometrical constraints, not the least of which was the need for the kicker plates to serve as rails for the NMR mapping trolley, the mechanical design was made, and the resulting field was calculated using OPERA. The calculated field was input into our particle tracking routine (discussed below) and the storage efficiency was found to be very close to that obtained with a perfect field. Because of the large phase-space mismatch between the inflector and the storage ring, our requirements on beam losses are much different from the usual situation where good field uniformity would be essential for good injection efficiency.

OPERA was also used to estimate the residual eddy currents in the vacuum chamber walls and the kicker plates themselves. We used the measured current as the current input to the kicker plates normalized with the appropriate factors. The calculated transient magnetic field from the eddy currents is compared directly to the measured eddy currents in the next section. Note that taking into account the total length of the kicker ($3 \times 1.76 \text{ m}^2$) compared to the ring circumference of 45 m, a 13 mG residual B -field corresponds to 0.1 ppm of $\int \vec{B} \cdot d\vec{l}$ around the entire ring.

In addition to aluminum for the kicker electrode material, copper and titanium were considered. It was found that Al was the best under our experimental conditions. For example, similar calculations with OPERA show that when 0.5 mm thick plates made of titanium are used, the eddy currents from the plates dominate. This results in very high, inhomogeneous residual B -fields, $\sim 100 \text{ mG}$ at $20 \mu\text{s}$, which become less than 13 mG only after $45 \mu\text{s}$ following muon injection. Both the Ti and Cu prototype electrodes were

²OPERA, Electromagnetic Fields analysis Program, Vector Fields Ltd., 24 Bankside, Oxford OX5 1JE, England.

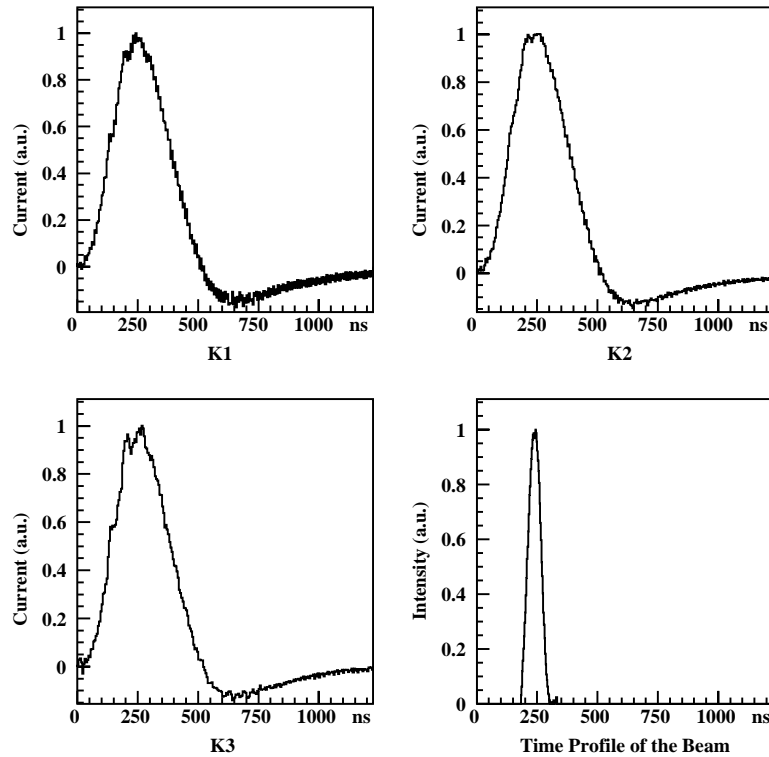


Fig. 10. A sample kicker current-waveform (in arbitrary units) from each of the three modulators (K1–K3) at 95 kV. The fourth figure shows a pulse from a thin beam scintillator which gives the time distribution of the injected beam.

unsatisfactory mechanically, so it was indeed fortunate that Al was the optimum electrode material. The calculations and measurements for Al are discussed below.

4. Measurement of the kicker B-field

The time dependent magnetic field of the kicker was measured in the prototype unit using the Faraday effect: the phenomenon that a changing magnetic field will result in a time dependent rotation of the polarization vector of a laser beam when it transits a dielectric material. In this section the Faraday magnetometer will be described, and the transient magnetic fields measured with it will be compared to the OPERA calculations.

Polarized light that propagates in a dielectric material in the presence of a magnetic field has its

polarization state rotated by an angle

$$\theta = VB\ell \quad (5)$$

where V is the Verdet constant of the material, B is the magnetic field *along* the light propagation direction and ℓ is the total light path in the material. The sense of rotation given by Eq. (5) depends only on the direction of the magnetic field and not on the direction of the light propagation. For a material with a positive value of Verdet constant, the rotation follows that of a right-handed screw moving in the direction of the magnetic field.

By detecting the angle θ as a function of time one can measure the changing magnetic field when V and ℓ are known. The merit of this method is that there are no metallic parts present but only dielectric materials so that the measuring instrument itself does not influence the remnant

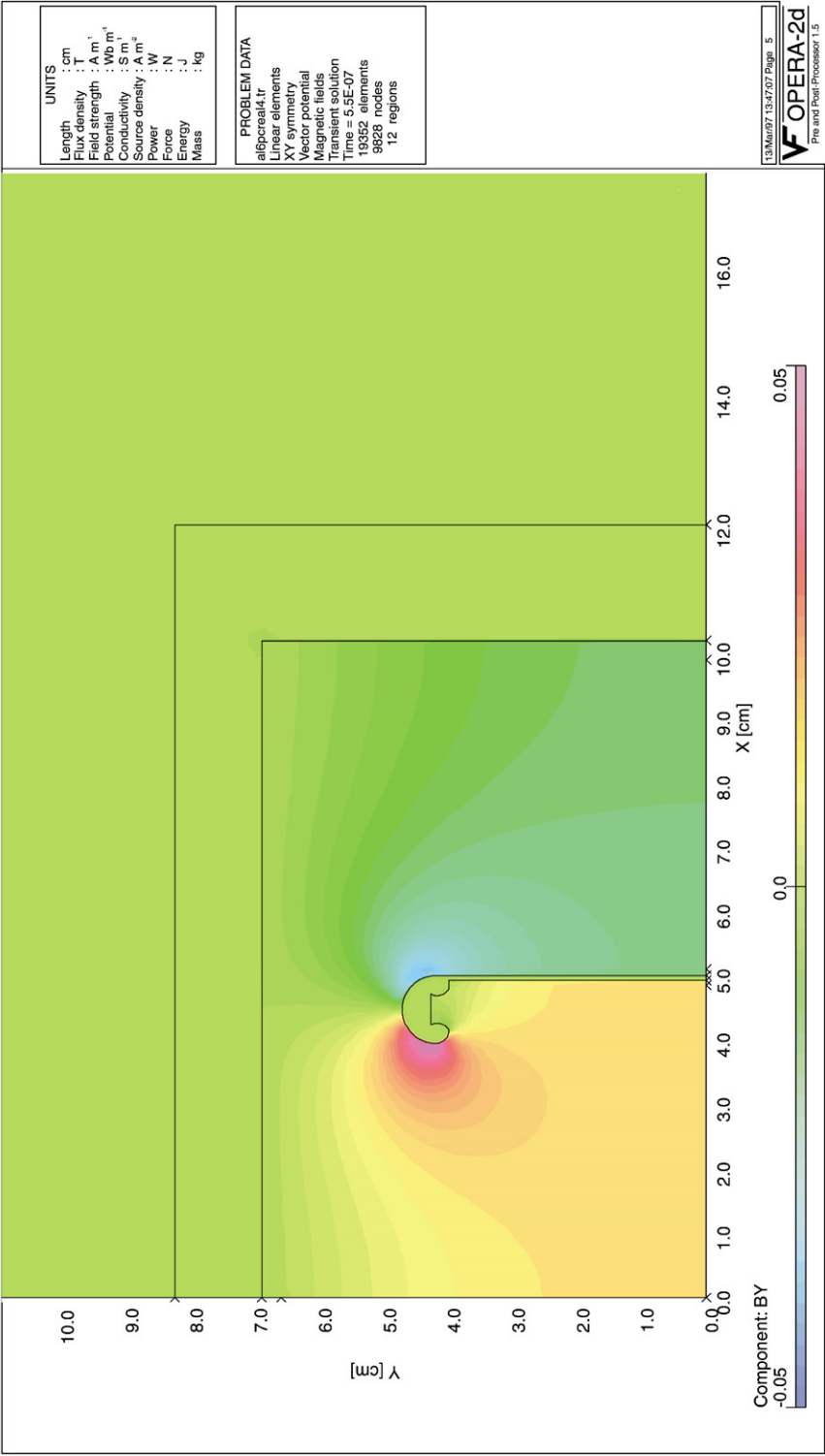


Fig. 11. The vertical B -field distribution calculated from OPERA. The symmetry is four-fold with only the upper right-hand quadrant shown. The lower left corner represents the center of the muon storage region.

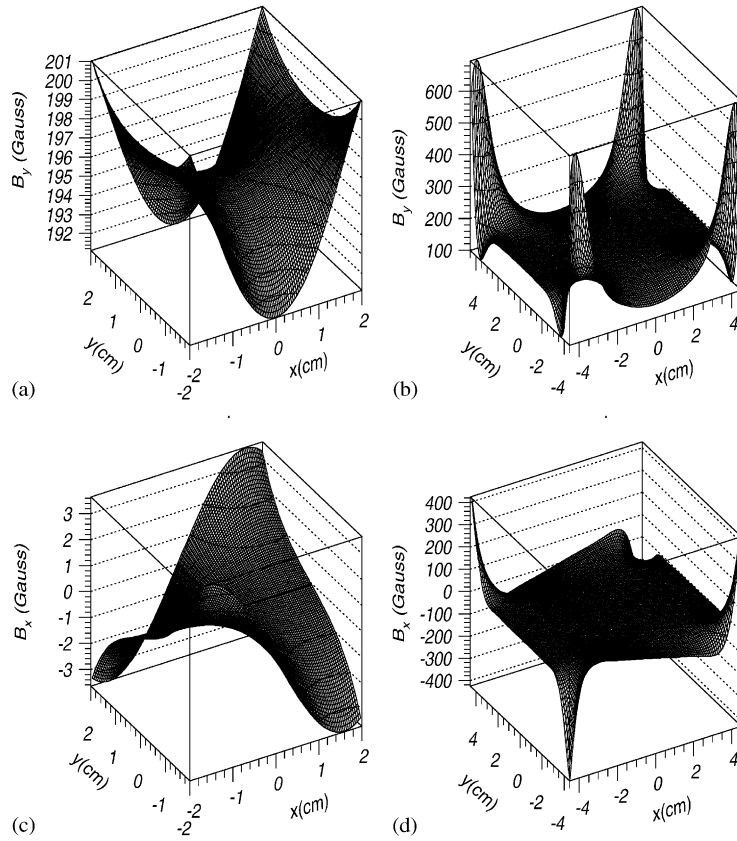


Fig. 12. The calculated radial (B_x) and vertical (B_y) kicker magnetic fields. (a) The vertical kicker field in the central 2×2 cm² region. (b) The vertical kicker field over the entire storage region. (c) The horizontal kicker field in the central 2×2 cm² region. (d) The horizontal kicker field over the entire storage region.

magnetic field (RMF). In addition, this technique has a large dynamic range and its time response is fast, limited only by the time constants of the detection electronics. The tests were performed without the large static dipole magnetic field of the storage ring present, since our studies have shown that its effect on the eddy currents is negligible.

The setup used for the measurements is shown in Fig. 13. A green laser, which provided ≈ 50 mW of continuous wave Ar⁺ laser light with $\lambda = 514.5$ nm was operated at the 10 mW level. Following the laser there is a periscope (PS) for adjusting the height of the laser beam, and a Galilean telescope (GT) for minimizing the light

spot size at the TGG crystal³ site. The light is polarized by the polarizer P and then it enters the TGG crystal which is placed between the kicker plates. The Verdet constant of the crystal in the green is $V = -206$ rad T⁻¹ m⁻¹. The crystal is a cylinder of 3 mm diameter and 12 mm length. The main dipole (static) magnetic field of 1.45 T would be in the vertical direction, parallel to the axis of

³ A TGG is an artificially grown crystal with a big Verdet constant, i.e. for the same magnetic field you get large rotation without compromising the laser light quality. The crystal used in the tests was provided by Optics For Research, Box 82, Caldwell, NJ 07006.

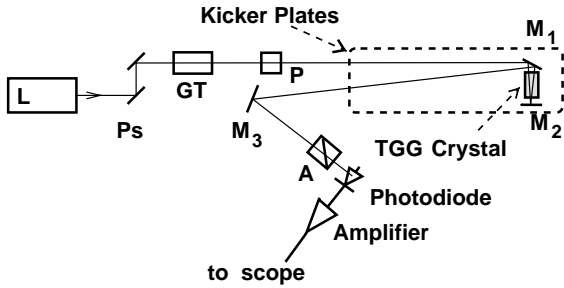


Fig. 13. A side view of the Faraday effect experimental setup. The side view of the kicker plates are shown as a dashed rectangle. The symbols are: L—Laser; Ps—periscope; M—mirror; A—polarization analyzer; P—polarizer; GT—Galilean telescope, (see text).

the crystal. The light is reflected into the crystal by a mirror ($M1$) and upon exiting the crystal is reflected back through the crystal by another mirror ($M2$). The mirror ($M3$) catches the returning ray and directs it to the analyzer (A) which is set for best extinction, σ^2 . For crossed polarizers, extinction is defined as the ratio of the light that escapes the second polarizer (also known as the analyzer), over the light intensity before the second polarizer. After the analyzer most of the laser light gets reflected away, and only a small fraction of it reaches the silicon photodiode, which has a spectral sensitivity of 0.27 A/W and a transimpedance gain of 4×10^4 V/A. The detector bandwidth is 125 MHz. The light intensity I on the photodiode is

$$I = I_0[\sigma^2 + \sin^2(\alpha + \theta)] \quad (6)$$

which for α and $\theta \ll 1$ becomes

$$I \simeq I_0[\sigma^2 + 2\alpha\theta + \theta^2] \quad (7)$$

where I_0 is the light intensity before the analyzer and the extinction factor $\sigma^2 \approx 10^{-5}$ for the polarizer crystals used in the tests.

The angle α is the static rotation introduced to the system in order to linearize the effect and to improve the signal to noise ratio. For the best signal to noise ratio and shot noise limit, it turns out that $\alpha \geq \sqrt{\sigma^2}$. In practice we used $\alpha \gg \sqrt{\sigma^2}$. With the intentional misalignment typically used of $\alpha \approx 0.140 - 0.210$ rad. Eq. (7) can be separated

into a DC and a time dependent component

$$I_{DC} = I_0(\sigma^2 + \alpha^2) \approx I_0\alpha^2 \quad (8)$$

and

$$I_\theta(t) = I_0[\theta^2(t) + 2\alpha\theta(t)]. \quad (9)$$

From Eqs. (7) and (5) we find the Faraday rotation angle θ (which can be positive or negative)

$$\theta = -\alpha \left\{ 1 - \sqrt{1 - \frac{I_\theta}{I_{DC}}} \right\} \approx -\frac{\alpha}{2} \frac{I_\theta}{I_{DC}} \quad (10)$$

the second equality being true when $(I_\theta/I_{DC}) \ll 1$.

The measurement of the magnetic field at 95 kV, 4200 A at the kicker in the burst mode (as required by the experiment) is shown in Fig. 14. The amplitude of the magnetic field is 165 G with an absolute error of 15%. We took field measurements with the crystal located both at the center of the storage region, i.e. $(x, y) = (0, 0)$, and at a location offset horizontally by 2.5 cm, i.e. $(x, y) = (2.5 \text{ cm}, 0)$. With the crystal length of 12 mm, the total light path $\ell = 24$ mm, and for the crystal used we observed -4.94 rad T^{-1} with a 5% accuracy. The field shown in Fig. 14 is taken with the crystal in the offset location.

When using the measured current as input, the OPERA simulation gave a magnetic field waveform which agrees in shape and absolute amplitude to better than 10% with the magnetic field measured with the Faraday effect.

The residual magnetic field is measured with the same system as above, but this time we used AC coupling on the oscilloscope and increased its gain.

The RMF measurement requires observing a very small signal 20 μs after the large primary kicker pulse. To test for saturation effects, the electronics system (1801 photodiode and pre-amplifier from New Focus and the 9314 series LeCroy oscilloscope) has been tested with a fast LED light signal to measure its recovery time. The peak signal was a 400 ns wide 1 V amplitude square pulse (a few times higher than the peak voltage value at the peak of the pulsed magnetic field), and the system recovered adequately without after-pulsing in less than 20 μs .

The measured RMF is shown in Fig. 15, and can be seen to be a rapidly dying oscillation following the main pulse. The RMF after 30 μs

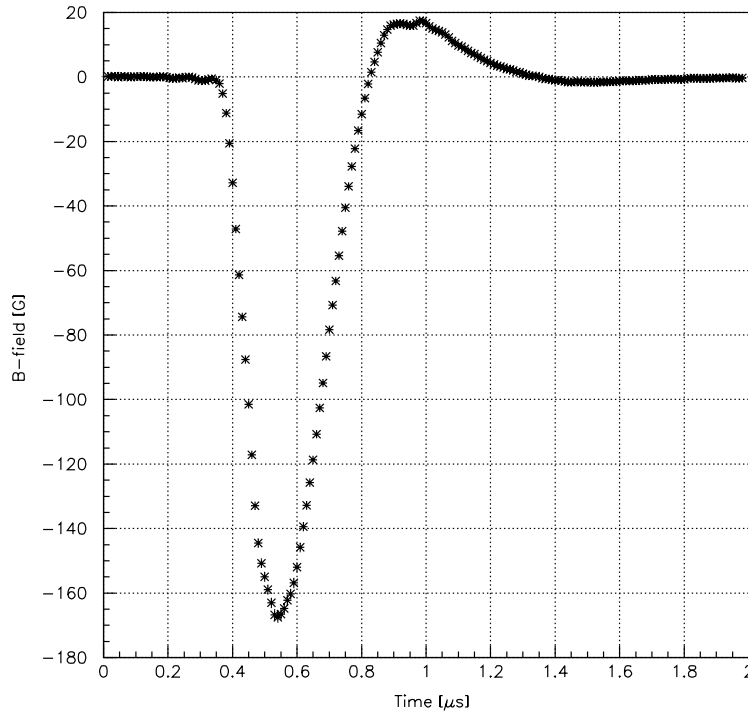


Fig. 14. The pulsed magnetic field produced by the muon kicker measured with the optical polarimeter with the crystal at the $(x, y) = (2.5 \text{ cm}, 0)$ location. The kicker was fired at 95 kV, producing 4200 A at the kicker plates.

contributes less than 0.1 ppm to the $\int \vec{B} \cdot d\vec{z}$ seen by the muon beam.

5. Calculations of the injection efficiency

The $g - 2$ tracking code⁴ was used to calculate injection efficiencies under a number of assumptions. The injected muons (input to the tracking code) were generated by BETRAF [10]. Fig. 16(a) shows the momentum distribution of the injected muons, which were distributed in time according to a Gaussian with $\sigma = 20 \text{ ns}$.

The injection efficiency was calculated with an ideal pulse and uniform magnetic field, as well as

for the LCR waveform which was obtained from the modulator circuits. Assuming an ideal pulse and a uniform magnetic field between the kicker plates, simulations predicted an injection efficiency of $8.6(\pm 0.3)\%$. With the vertical magnetic field calculated for the electrode geometry shown in Fig. 5, the efficiency was calculated to be $8.4(\pm 0.3)\%$, the same to the accuracy of the calculation. Thus 8.6% is the maximum achievable injection efficiency, which we call the “ideal kicker”. For comparison, the maximum achievable injection efficiency with our kicker waveform was calculated to be $7.4(\pm 0.3)\%$.

The injection efficiency for the simplest case of an ideal (square) pulse and an ideal magnetic field (0.1 Tm when integrated over the length of the kicker) was 8.6%. When a realistic field was used, the injection efficiency remained the same within errors. Fig. 16(b) shows the injection efficiency as a function of strength of ideal kicks. For this calculation, the end of the

⁴Efsthadiadis, B. Lee Roberts, Yannis K. Sermert-zidis, Tests of New Version of The Tracking code, ($g - 2$) note #283, 14 Feb. 1997. The equations of motion taken from M. Berz (Nucl. Inst. and Meth. A 298 (1990)473) were integrated by a Burlish-Stoer integration routine.

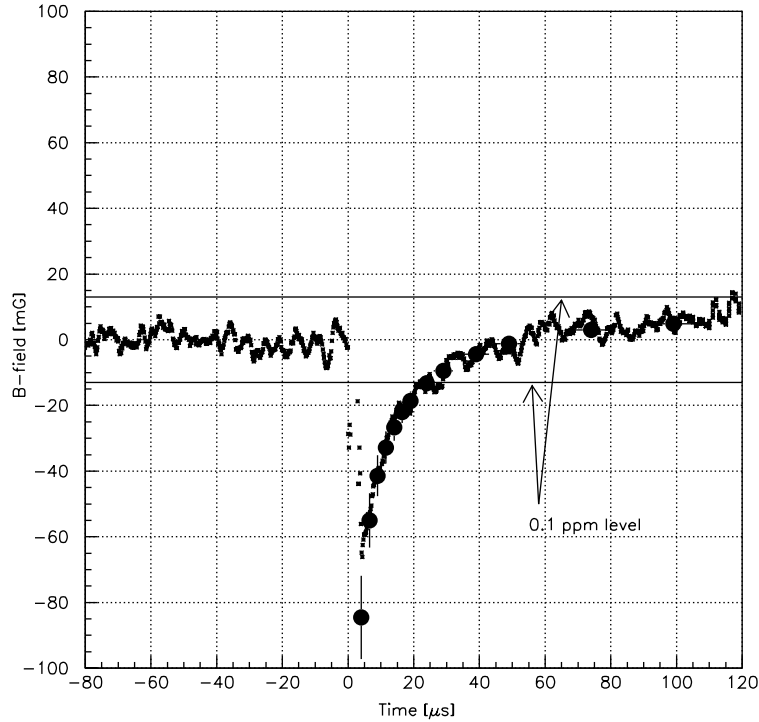


Fig. 15. The magnetic field produced mainly by eddy currents on the kicker plates as measured by the optical polarimeter with the crystal at the $x, y = (2.5 \text{ cm}, 0)$ position. The kicker was fired at 95 kV, producing 4200 A at the kicker plates. The solid lines show the range $\pm 0.1 \text{ ppm}$ on $\int \vec{B} \cdot d\vec{z}$. The filled circles correspond to simulations with OPERA which used the measured current pulse as input.

inflector (injection point) was at $x = 77 \text{ mm}$ radially outward from the center of the storage region. The mean horizontal and vertical injection angles were zero. Fig. 16(c) shows the injection efficiency as a function of radial position of the injection point for two different ideal kicks. Fig. 16(d) shows the injection efficiency as a function of the horizontal slope of the inflector for an ideal kick of 0.1 Tm and the inflector end at $x = 77 \text{ mm}$.

From Fig. 16(c) one sees that for each distance from the storage region, there is an optimal kick magnitude. Furthermore, from Fig. 4, one can see that as the inflector center moves closer to the storage ring, the magnitude of the necessary injection kick goes down. One also sees that as one moves the inflector center radially outward, the maximum injection efficiency falls. Because of

the inflector/support/cryostat structure, we are forced to have the inflector center at $\geq 77 \text{ mm}$ radially outward from the center of the beam storage ring.

In developing the design of the kicker, many calculations were carried out to determine which parameters were essential and which could be compromised to achieve a working design. From prototype tests it became apparent early on, that the shortest base pulse-width obtainable was about 400 ns , and the maximum voltage without substantially increasing the inductance (see Eq. (4)) was 100 kV . Nevertheless, these calculations gave us some confidence that the device which we could build would work, and that a substantial number of muons could be stored even though the width of the kicker pulse is substantially broader than the cyclotron period of 150 ns . This hope has been

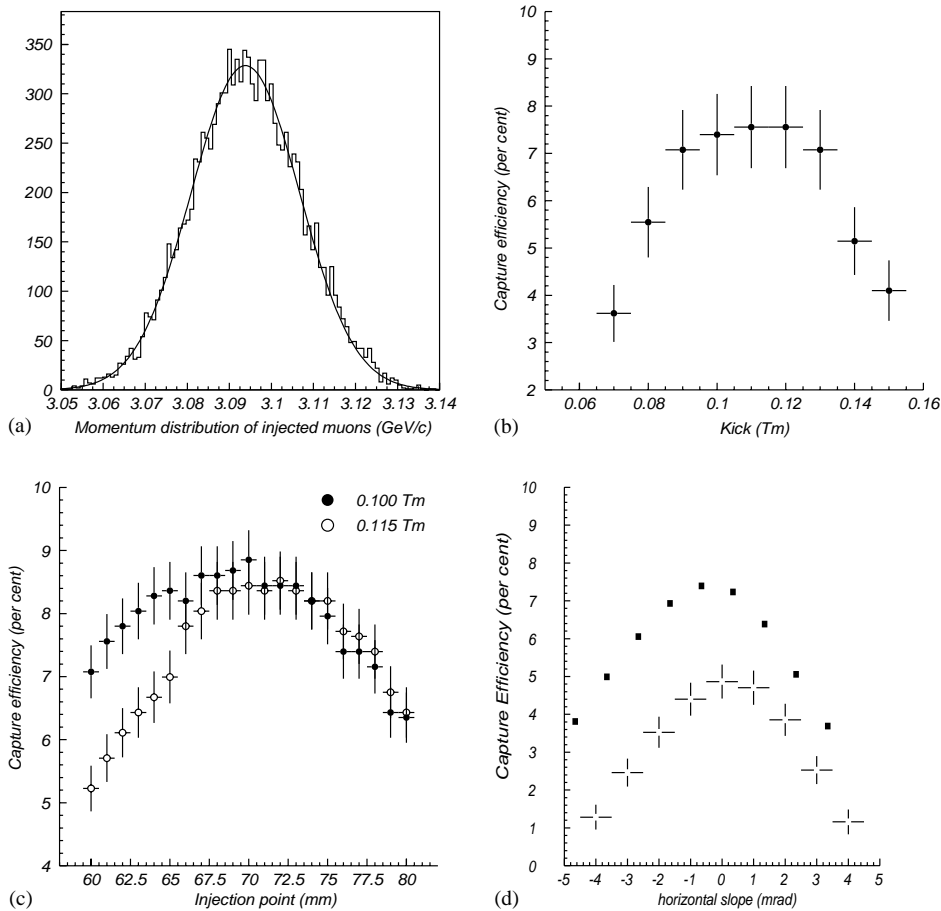


Fig. 16. (a) Momentum distribution of injected muons in GeV/c. The line is a Gaussian fit with a centroid at 3.094 GeV/c (the magic momentum) and a σ of 0.013 GeV/c. (b) Injection efficiencies as a function of ideal kicks (integrated over the length of the kicker.) The injection point was at $x = 77$ mm from the center of the storage region, and the inflector slopes (horizontal and vertical) were 0 mrad. In the case of ideal kicks the injected muons get kicked only once (in the first turn). (c) Injection efficiencies as a function of radial injection position for tow different ideal kicks. The inflector slopes (horizontal and vertical) were 0 mrad. (d) Injection efficiencies as a function of horizontal slope of the inflector.

shown to be real by our subsequent experience. Only the most important results from these calculations are given in this paper.

After an operational prototype was constructed and tested, the measured pulse was parameterized and put into the tracking code. The first measurements were performed at 65 kV and the waveform was scaled for other voltages by assuming that the shape does not change. This was shown to be a reasonable assumption once the EEV CX1699 thyratron was obtained which permitted an

operating voltage up to 100 kV. In Figs. 9 and 10 the prototype pulse shape can be compared to the operational kicker waveforms. Fig. 17 shows the calculated capture efficiency for the measured pulse shape as a function of kicker high voltage. We concluded that while less than ideal, the capture efficiency possible with our waveform and a peak voltage of 90–95 kV would provide substantially more stored muons, with much less background than pion injection.

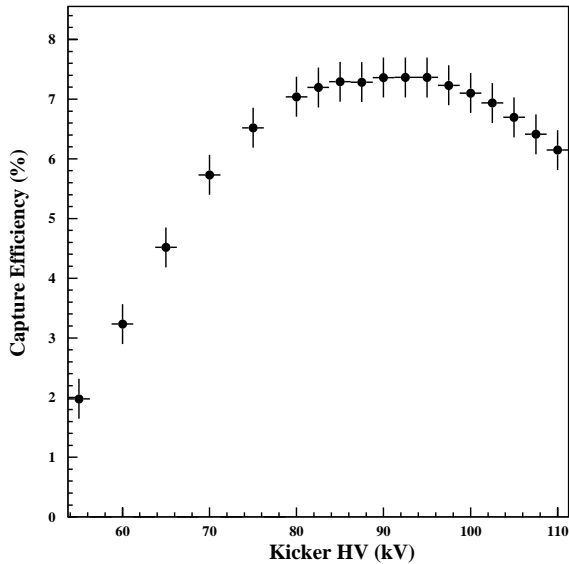


Fig. 17. Calculated capture efficiency vs voltage for the measured waveform. The maximum efficiency is 7.4%.

6. Discussion and conclusions

The fast muon kicker described in this paper has been essential to the ability of the muon ($g - 2$) collaboration to obtain a large volume of high quality data. These data will lead to a measurement of the muon anomaly a_μ to a relative level of precision on the order of half of a part per million or better. The results thus far have led to widespread interest in the physics community, and will play an important role in defining the future of the standard model and its extensions. While pushing the state of the art in many aspects of its design, this kicker system has now worked reliably for $\sim 4 \times 10^7$ pulses. While the phase space population is not ideal, it does not limit the accuracy of the experiment.

There has been some talk of a next generation muon $g - 2$ experiment at the Japan Hadron Facility under construction at the JAERI/Tokai site. If one were to build a next generation kicker, several important lessons would be carried forward. The kicker inductance limited the peak current of the device, and a next generation would certainly require a new look at all components of

the kicker. For example, the vacuum high-voltage feed-through would certainly need to be re-designed, and with care, one might reduce the inductance in an improved device. One way of reducing the uncertainty on a_μ would be to reduce the aperture of the storage ring, and increase the flux of stored particles. A smaller kicker-plate spacing would simplify the kicker design. One would also need to run the kicker for more than 12 pulses per cycle, and perhaps at a higher repetition rate. With the 12-bunch mode of AGS running, we fired our kicker every 33 ms until all the bunches in the AGS had been used. It then took about 2 s for the AGS to ramp up to full energy with the next 12 bunches. We see no problem in increasing the number of pulses per accelerator cycle by a factor of two or three.

Acknowledgements

We are grateful to Dr. Derek Lowenstein and the staff of the Collider Accelerator Department for their help and support in the planning and construction of this device. Valuable advice was given by Andy Soukas. We acknowledge the important role of Robert Vere, Leo Dumais and the staff of the Boston University Scientific Instrument Facility where the mechanical components were fabricated. Don von Lintig's careful assembly of the components was essential to the success of this device. We also gratefully acknowledge the contribution of Peter von Walter of the University of Heidelberg Physikalishes Institut who provided several electronic modules used in the control circuit. We thank V. Goklani for his help in testing early versions of the prototype. E.B. Forsyth, G.C. Pappas and W.Q. Feng carried out early design studies which indicated the magnetic kicker might work. F. Krienen proposed an alternative electrostatic design which elucidated many of the important issues of the fast muon kicker. We also thank the many members of the ($g - 2$) collaboration who made useful suggestions and criticisms during the kicker development. This work was supported in part by the US Department of Energy and the US National Science Foundation.

References

- [1] J. Bailey, et al., Nucl. Phys. B 150 (1979) 1.
- [2] R.M. Carey, et al., Phys. Rev. Lett. 82 (1999) 1632.
- [3] H.N. Brown, et al., Phys. Rev. D 62 (2000) 091101;
H.N. Brown, et al., Phys. Rev. Lett. 86 (2001) 2227;
G.W. Bennett, et al., Phys. Rev. Lett. 89 (2002) 101804.
- [4] F. Combley, E. Picasso, Phys. Reports C 14 (1974) 1.
- [5] R. Prigl, et al., Nucl. Instr. and Meth. A 374 (1996) 118;
X. Fei, V.W. Hughes, R. Prigl, Nucl. Instr. and Meth. A 394 (1994) 349.
- [6] S.A. Sedykh, et al., Nucl. Instr. and Meth. A 455 (2000) 346.
- [7] G.T. Danby, et al., Nucl. Instr. and Meth. A 457 (2001) 151.
- [8] F. Krienen, D. Loomba, W. Meng, Nucl. Instr. and Meth. A 283 (1989) 5.
- [9] H.N. Brown, et al., Nucl. Instr. and Meth. (2003), in preparation
- [10] J. Sandweiss, I.O. Skillicorn, M.S. Webster, The program BETRAF, in 1962, BNL Bubble Chamber Group Report H-11, was updated by H.N. Brown 1982, and by A. Carroll, 1983.